Proc. U.S.-Korea Workshop on Smart Structural Systems, Eds. C.-K. Choi, F.Y. Cheng and C.-B. Yung, pp. 43-50, Pusan, Korea, 23-24 August 2002

On magnetostrictive materials and their use in smart material transducers

Marcelo J. Dapino
Department of Mechanical Engineering
The Ohio State University
2091 Robinson Laboratory
Columbus, OH 43210-1107, USA
Ph.: +(614) 688-3689
E-mail: dapino.1@osu.edu

Abstract

Although magnetostrictive materials have been successfully employed in a wide variety of dynamical applications, for example noise and vibration control of mechanical equipment, their implementation in infrastructural systems is sparse. Technologies currently favored for infrastructural applications include, among others, hydraulic actuation and piezoelectric sensing. These technologies have reached a degree of technical maturity and in some cases, cost effectiveness, which justify their broad use in infrastructural applications. Advanced civil structures present new challenges in the areas of wireless communications, reliability, and high-authority actuation which motivate the need to explore new methods and materials recently developed in other fields. This paper provides an overview of a class of materials that because of the large force, displacement, and energy conversion efficiency that it can provide is being considered in a growing number of quasistatic and dynamic applications. Since magnetostriction involves a bidirectional energy exchange between magnetic and elastic states, magnetostrictive materials provide mechanisms both for actuation and sensing. This exchange can lead to broadband and multifunctional devices. Furthermore, recent materials science advances have facilitated materials of diverse geometries, notably particles for use in active sensoriactuator composite concepts. The ability to harness the favorable properties of magnetostrictive materials highly depends upon the ability to model magnetic hysteresis. The deleterious effects due to hysteresis, specifically phase and magnitude nonlinearities in magnetic field vs. strain relationships, can be substantially ameliorated through scalable models constructed from physical principles. This paper provides an overview of materials, methods and applications with the goal to inspire novel solutions based on magnetostrictive materials for the design and control of advanced infrastructural systems.

1 Introduction

The study of magnetostriction began in 1842 when James P. Joule first observed that a sample of iron changes its length when magnetized with a magnetic field. The term magnetostriction refers to any change in dimension of a magnetic material caused by a change in its magnetization. Changes in magnetization result from magnetic moment rotations, which can be brought about by the application of magnetic fields, heat, or stresses. Figure 1 illustrates the Joule magnetostriction $\Delta L/L$ of a cylindrical sample, resulting from a magnetic field being applied along the longitudinal axis. The Joule magnetostriction is commonly employed in actuator and sensor applications. While most magnetic materials exhibit Joule magnetostrictions, only a small number of compounds containing rare earth elements provide strains in excess of 1000×10^{-6}. These large strains are a direct consequence of a strong magnetoelastic coupling arising from the dependency of magnetic moment orientation with interatomic spacing. Referring again to Figure 1, if the magnetostriction is positive, the sample elongates irrespective of the direction of rotation of the magnetic moments, and the diameter is reduced such that the volume remains constant. If the magnetostriction is negative, the sample

length decreases, and the diameter increases. A symmetric magnetostriction curve is then obtained as the magnetic field is cycled. If a uniaxial stress is applied, interatomic displacements lead to magnetic moment reorientation and a subsequent change in total magnetization. This effect provides a mechanism for sensing.

Because magnetostriction is an inherent property of magnetic materials, it does not degrade over time as can be the case with some piezoelectric substances. Furthermore, newer magnetostrictive materials provide strains, forces, energy densities, and coupling coefficients which compete advantageously with more established transducer technologies such as those based on piezoelectric materials. A number of design and modeling issues, however, complicate the implementation of magnetostrictive materials. For instance, due to the required solenoid and related magnetic circuit components, magnetostrictive transducers are usually larger and bulkier than their piezoelectric or electrostrictive counterparts. Hence a primary application for magnetostrictive materials is vibration control of heavy structures. One additional consideration is that the most technologically advanced magnetostrictive compounds are costly to manufacture, as advanced crystalline transducer drivers must be manufactured through crystal growth techniques that produce directional solidification along the drive axis, in combination with precision machining of laminations, final diameters, and parallel ends of cut-to-length pieces.

From a device implementation standpoint, magnetostrictive materials exhibit significant nonlinearities and hysteresis to a degree which other smart materials, for instance electrostrictives, typically do not. The deleterious effects due to these behaviors can be circumvented through feedback control techniques. However, the development of broadband feedback control solutions that do not degrade in performance over a large performance range has been elusive in many magnetostrictive systems, because in these systems the efficacy of real-time monitoring and feedback control is diminished by noise inherent to hysteresis, thermal creep, and strong material property variations. One effective means of accounting for and limiting the deleterious effects of these issues is through the development of feedforward loops utilizing constitutive laws describing material behavior in terms of its inherent physical properties. Important advances on the modeling of magnetostrictive materials and structures have taken place recently, and as transducer designers find opportunities to develop new applications, model completeness and accuracy will surely follow. In addition, recent advances in materials science research have enabled more capable magnetostrictive materials in various forms, including amorphous or crystalline thin films, magnetostrictive particle-aligned polymer matrix composite structures, and sintered powder compacts suitable for mass production of small irregular shapes.

In the following sections, concepts concerning magnetostrictive materials, modeling considerations, and transducer implementation are discussed. In Section 2, an overview of magnetostrictive materials is provided, followed by a discussion of material behavior in Section 3. Section 4 is devoted to Joule magnetostriction, while other magnetostrictive effects are discussed in Section 5. Finally, a discussion on current transducer designs is presented in Section 6.

2 MATERIALS OVERVIEW

During the early 1960's, a breakthrough in magnetostrictive materials occurred with the discovery of the largest-known magnetostriction in the rare earth elements terbium and dysprosium. The strains in these elements are of the order of $10{,}000\times10^{-6}$, or three orders of magnitude larger than those of nickel, but they are achieved at cryogenic temperatures. The temperature limitation and the fact that the field of piezoelectricity was gaining technical maturity hindered the development of magnetostrictive materials and led in the early 1970's to a search for a new class of transducer materials capable of high room-temperature strains. Highly magnetostrictive rare earths (R), principally samarium (Sm), terbium (Tb) and dysprosium (Dy), were combined with the magnetic transition metals nickel, cobalt and iron by direct compound synthesis and by rapid sputtering into amorphous alloys. In contrast to the normal Curie temperature behavior of the R-Ni and R-Co compounds, the R-Fe compounds exhibit an increase in the Curie temperature with increasing rare earth concentration [8]. This unusual property facilitates huge room temperature magnetostrictions, of up to $3{,}000\times10^{-6}$, particularly in the $TbFe_2$ compound. However, because magnetostriction originates in the strain dependency of magnetic anisotropy, the large magnetostriction in these compounds is obtained at the expense of large anisotropies. This poses a technological limitation in that impractical large fields of over 2 MA/m are needed to bring these compounds to saturation.

Partial substitution of dysprosium for terbium in the $TbFe_2$ system resulted in improved magnetostriction and anisotropy properties. The resulting pseudobinary compound $Tb_{0.3}Dy_{0.7}Fe_{1.9-1.95}$ has been available

commercially since the 1980's under the name Terfenol-D (**Ter** =terbium, **Fe** = iron, **N** = Naval **O** = Ordnance **L** = Laboratory, **D** = dysprosium). The highest room-temperature magnetostriction for Terfenol-D is 1600×10^{-6} at a moderate saturation field of 0.16 MA/m, but even larger magnetostrictions of up to 3600×10^{-6} are possible when this material is employed in transducers driven at mechanical resonance. The utility of Terfenol-D as a rugged, high power transducer driver has been increasingly recognized in recent years. At present, Terfenol-D is used in active noise and vibration control systems, low frequency underwater communications (sonar), linear and rotational motors, ultrasonic cleaning, machining and welding, micropositioning, and the detection of motion, force and magnetic fields. Terfenol-D is currently available in a variety of forms, including monolithic rods [1, 2], particle-aligned polymer matrix composites [3, 4, 5] and thin films [6, 7]. Because of the large magnetostriction anisotropy and strong magnetoelasticity, Terfenol-D and other pseudobinary rare earth-iron compounds can be synthesized to exhibit a broad range of properties [8].

A second new magnetostrictive material was introduced in 1978 which is based on amorphous metal, produced by rapid cooling of iron, nickel, and cobalt alloys together with one or more of the elements silicon, boron, and phosphorus. These alloys are known commercially as Metglas (metallic glass) and are commonly produced in thin-ribbon geometries. Because of the extremely high coupling coefficients ($k > 0.92$), Metglas is a prime candidate for sensing applications in which a mechanical motion is converted into an electrical current or voltage [2].

The latest research on magnetostrictive materials includes the development of new compounds to minimize magnetic anisotropy and hysteresis, and new manufacturing techniques to produce Terfenol-D thin films efficiently [9]. Substantial materials science advances have been achieved with the quaternary compounds Terfenol-DH, which are produced by substitution of holmium for terbium and dysprosium [10]. In addition, new manufacturing techniques are enabling the production of multi-layered driver rods which will lead to reduced dynamic losses, thus facilitating the operation over a broad frequency spectrum into the MHz range. The ferromagnetic shape memory alloys are another class of smart materials which hold much promise due to the large strains that they can provide. While the nickel-titanium alloy commercially known as Nitinol features large recoverable strains in the order of $60{,}000\times10^{-6}$, it suffers from inferior dynamical response. The possibility of combining the desirable aspects of shape memory with magnetostriction through actuating an SMA with a magnetic field is currently being investigated. Promising candidate materials are the Ni_2MnGa system and the Fe-based invars, which exhibit, in principle, the desired characteristics. Further details on the Ni-Mn-Ga alloys can be found in [11, 12].

3 Material Behavior

3.1 Magnetic anisotropy

Magnetic anisotropy refers to the dependency of magnetic properties on the direction in which they are measured. It can be of several kinds, including crystal, stress, shape and exchange anisotropy. Of these, however, only crystal anisotropy is a material property. In many crystalline materials, the magnetic moments do not rotate freely in response to applied fields, but rather they tend to orient along preferred crystallographic directions. This phenomenon is called the magnetocrystalline (or crystal) anisotropy, and the associated anisotropy energy is the energy required to rotate the magnetic moments away from their preferred directions. Crystal anisotropy energy and magnetostriction are closely related effects; if the anisotropy were independent of the state of strain, there would be no magnetostriction [14].

While accurate models for crystal anisotropy and its relation with the magnetization process exist for the simple cases of cubic and hexagonal crystals [15, 16], models for complex crystal structures often rely on simplifying assumptions which reduce the analysis to the simpler cases. For example, in transducer design it is often useful to consider operating regimes in which stress anisotropy dominates crystal anisotropy. This simplifies the modeling of complex materials, for example Terfenol-D whose crystals are grown in dendritic twin sheets oriented in the $[11\overline{2}]$ direction (see Figure 2 and [1]). At room temperature and moderate stress, Terfenol-D exhibits $\lambda_{111} = +1600 \times 10^{-6}$, so a compressive stress applied along the $[11\overline{2}]$ direction produces a significant decrease in the internal energy of the crystal at right angles to the applied stress. Conversely, even though the anisotropy coefficient of Terfenol-D varies significantly depending on temperature and stoichiometry ($K_1 = -4$ to -50 kJ/m^3 [3, 17]), it is nonetheless large enough to resist

energy changes by favoring magnetic moment alignment along the <111> directions. It is then inferred that a sufficiently large compressive stress will raise the elastic energy above that of the crystal anisotropy, shifting the preferred orientation of domains to the <111> magnetic easy axes which are perpendicular to the easy crystal growth direction, that is the $[11\overline{2}]$ axis. Under large compressive stress the population density in these two orientations will increase, and a magnetic field applied along the $[11\overline{2}]$ direction will produce nearly isotropic 90° rotations. In addition, under compression, as large populations of magnetic moments align along directions perpendicular to the stress direction, the demagnetized length decreases to a minimum and the saturation magnetostriction potential increases to a maximum. The 90° rotations subsequently provide the maximum possible magnetostrictions. In summary, materials that have positive magnetostrictions exhibit enhanced magnetostriction under moderate compression. Too little or too much compression degrade the magnetostriction. In nickel, which has a negative magnetostriction coefficient, the effect is reversed and enhanced magnetoelasticity is obtained from tensile stresses. Further details regarding crystal anisotropy can be found in [18, 19, 20]. The manner in which the precompression is implemented in transducer applications is discussed in Section 6.

3.2 Domain processes and hysteresis

The changes in magnetization which result from an applied magnetic field can be either reversible or irreversible. Reversible magnetization changes are energetically conservative and occur for small field increments in which the material can return to the original magnetic state upon removal of the field. Irreversible magnetizations are dissipative since external restoring forces are needed to bring the magnetism to its original state, such as when large fields are applied. In applications, both types of processes take place during the magnetization. The magnetization, either reversible or irreversible, can be explained by considering two related mechanisms: the rotation of moments and the movement of domain walls. We note that the origin of domain walls lies in the domain structure characteristic of ferromagnetic materials below their magnetic phase transition temperature or Curie temperature, T_c (see Table 1 for values of T_c for several magnetostrictive materials). When a ferromagnetic material is cooled below its Curie temperature, the magnetic moments become ordered within magnetic domains. Each domain has all its moments aligned parallel producing a spontaneous magnetization M_s, but under no field the direction of M_s varies from domain to domain such that the bulk magnetization in the material averages to zero. This is illustrated with the randomly oriented regions of Figure 3(a).

When a small magnetic field H is applied, Figure 3(b), domains oriented favorably with respect to the field grow at the expense of the remaining domains and the main magnetization mechanism is domain wall motion. As the field is increased in Figure 3(c), entire domains rotate to orient with the easy $[11\overline{1}]$ axis. This produces a burst region in the M-H and ε-H curve in which small field changes produce large magnetization or strain changes. In the final stage shown in Figure 3(d), the material acts as a single domain as magnetic moments rotate coherently from the easy axis into the direction of the field. This produces saturation of the magnetization. Typical magnetization and strain loops are shown in Figure 4 which illustrate the burst region and saturation effects. From a design perspective, magnetic biasing as described later in Section 6 is used to center operation in the burst region for optimum performance.

For low magnetic field levels, partial excursions in the M-H or ε-H curve are approximately linear. However, hysteresis is always present to some extent. The hysteresis can be attributed to the irreversible impediment to domain motion by pinning sites, such as when domain walls move across twin boundaries in Terfenol-D. Modeling hysteresis and nonlinear behavior is currently a focal point in the design and control of magnetostrictive materials. Details on the topic of ferromagnetic hysteresis can be found in [14, 21, 22].

3.3 Material properties

Table 1 lists nominal material properties corresponding to several magnetostrictive materials of interest. The linear magnetomechanical coupling coefficient k quantifies the ratio of input energy which is available as output energy. Other properties include the elastic modulus E, saturation induction B_s, Curie temperature T_c,density ρ, and saturation magnetostriction λ_s. These properties typically vary, often substantially, during transducer operation [23]. Efficient transducer design requires an accurate assessment of material property behavior under varying operating conditions.

4 Joule Magnetostriction

The Joule magnetostriction pertains to the strain produced along the field direction and is the most commonly used magnetostrictive effect. Because this effect occurs at constant volume, there must be a transverse strain with opposite sign to that of the linear magnetostriction,

$$\lambda_\perp = -\frac{\lambda}{2}.$$

4.1 Isotropic spontaneous magnetostriction

When a ferromagnetic material is cooled below its Curie temperature, a transition from paramagnetism to ferromagnetism takes place and magnetic moments become ordered giving origin to a spontaneous magnetization M_s within domains. This process is accompanied by a spontaneous magnetostriction λ_0. It is in fact possible to derive a relationship between λ_0 and the saturation magnetostriction λ_s. To that end, we consider an isotropic material in the disordered state above T_c, which is therefore modeled with spherical volumes as shown in Figure 5(a).

As the material is cooled below T_c, spontaneous magnetization M_s is generated within magnetic domains along with the corresponding spontaneous magnetostriction λ_0. The domains are represented in Figure 5(b) by ellipsoids with spontaneous strain e. Since the material is isotropic, the magnetic domains are oriented randomly; each bears an angle θ with respect to the direction of measurement. The net magnetization is consequently zero, and the length in the direction of interest is given by [13]

$$e(\theta) = e\,\cos^2\theta. \tag{1}$$

Then, the average domain deformation on the onset of spontaneous magnetostriction is obtained by integration along all possible directions,

$$\lambda_0 = \int_{-\pi/2}^{\pi/2} e\,\cos^2\theta\,\sin\theta\,d\theta = \frac{e}{3}.$$

Spontaneous magnetostriction λ_0 is homogeneous in all directions, so the material has changed its dimensions but not its shape. On application of a magnetic field, the magnetic domains rotate and become aligned either parallel with the field or perpendicular to it, depending on whether the material exhibits positive or negative magnetostriction. Assuming positive magnetostriction, the domains rotate into the field direction as depicted in Figure 5(c). Near saturation, the material becomes a single domain and the total strain becomes e. Then, the total available saturation magnetostriction is given by the difference between e and λ_0,

$$\lambda_s = e - \lambda_0 = \frac{2}{3}\,e = 2\,\lambda_0. \tag{2}$$

This expression provides a method of measuring the spontaneous strain λ_0 by measuring λ_s. Methods to determine λ_s are discussed next.

4.2 Saturation magnetostriction

Assuming again for simplicity that the medium is isotropic, the saturation magnetostriction at an angle θ from the direction of the field is given by [13]

$$\lambda_s(\theta) = \frac{3}{2}\,\lambda_s\,(\cos^2\theta - \frac{1}{3}), \tag{3}$$

where $\lambda_s(\theta)$ is the saturation magnetostriction at an angle θ from the field and λ_s is the saturation value in the ideal demagnetized state, that is to say, when all possible directions are equally represented.

The saturation magnetostriction is then calculated from the difference between the maximum magnetostriction with the field parallel to a given direction ($\lambda_{s\parallel}$) and that with the field perpendicular to the given direction ($\lambda_{s\perp}$). Substituting $\theta = 0^\text{o}$ and $\theta = 90^\text{o}$ in (3) gives

$$\lambda_{s\parallel} - \lambda_{s\perp} = \lambda_s + \frac{1}{2}\,\lambda_s = \frac{3}{2}\,\lambda_s, \tag{4}$$

which defines λ_s independently of the demagnetized state.

Magnetostriction data from Clark [8] taken from polycrystalline $Tb_xDy_{1-x}Fe_y$ samples is reproduced in Figure 6. The data points correspond to $\lambda_{s\parallel} - \lambda_{s\perp}$ at room temperature and field values of $H = 10$ kOe (0.8 MA/m) and $H = 25$ kOe (2 MA/m). Near $x = 0.3$, the magnetostriction curve shows a peak in accordance with the near zero magnetic anisotropy observed at this composition. From the magnetostriction value at the peak, of about 1600×10^{-6}, equation (4) gives $\lambda_s = 1000 \times 10^{-6}$ which is a widely employed value for the saturation magnetostriction of Terfenol-D.

Anisotropy is present to some degree in all magnetic materials, and therefore the saturation magnetostriction needs to be defined in relation to the axis along which the magnetization lies. One exception is nickel, whose magnetostriction is almost isotropic (see Table 2). Recognizing that for cubic materials there are two independent magnetostriction constants λ_{100} and λ_{111}, the saturation magnetostriction assuming single crystal, single domain material is given by a generalization of equation (3) for isotropic materials,

$$\begin{aligned} \lambda_s &= \frac{3}{2}\lambda_{100}\left(\alpha_1^2\beta_1^2 + \alpha_2^2\beta_2^2 + \alpha_3^2\beta_3^2 - \frac{1}{3}\right) \\ &\quad +3\,\lambda_{111}\left(\alpha_1\alpha_2\beta_1\beta_2 + \alpha_2\alpha_3\beta_2\beta_3 + \alpha_3\alpha_1\beta_3\beta_1\right), \end{aligned} \tag{5}$$

where λ_{100} and λ_{111} are the saturation magnetostrictions along the <100> and <111> axes of the crystal. The cosines α_i $(i = 1, 2, 3)$ define the direction along which the magnetic moments are saturated, while the cosines β_i define the direction on which the saturation magnetization is measured. The saturation magnetostriction along the field direction is obtained by using $\alpha_i = \beta_i$ in equation (5), which leads to

$$\lambda_s = \lambda_{100} + 3\left(\lambda_{111} - \lambda_{100}\right)\left(\alpha_1^2\alpha_2^2 + \alpha_2^2\alpha_3^2 + \alpha_3^2\alpha_1^2\right). \tag{6}$$

It is noted that expressions (5) and (6) only apply to single domain materials. In the saturated state, the whole specimen consists of a single domain with its magnetization M_s aligned parallel to the applied field. However, when a domain structure is present such as in polycrystals, the magnetostriction can only be calculated by averaging the effects unless the domain structure is known specifically. Note that radically different domain configurations can give the same bulk magnetization and different magnetostrictions (see Figure 7). So, assuming that there is no preferred grain orientation, formula (6) simplifies further becoming

$$\overline{\lambda_s} = \frac{2}{5}\lambda_{100} + \frac{3}{5}\lambda_{111}.$$

Extensive magnetostriction data on the R-Fe_2 compounds can be found in [8], while calculations of λ_s in different crystallographic structures such as cubic, hexagonal and polycrystalline can be found in [16, 13, 21, 2].

4.3 Magnetostriction below saturation

While the saturation magnetostriction λ_s can be determined employing the methods just discussed, the magnetostriction between the demagnetized state and saturation is very structure sensitive so general constitutive relations for the magnetostriction are not plausible. However, an explicit solution exists for cases when the strains are due primarily to 90° domain rotations. In practice, these rotations occur in: (i) a single crystal with uniaxial anisotropy in which the field is applied in a direction perpendicular to the easy axis or (ii) a polycrystalline material in which the magnetic moments have been brought to complete alignment in a direction perpendicular to the applied field, such as Terfenol-D under extreme compression or nickel under tension. The latter case implies that the perpendicular stress energy is sufficient to dominate the crystal anisotropy, as discussed in Section 3.1. For that regime, combining equation (1) and $e = 3\,\lambda_s\,/\,2$ from equation (2) gives

$$\lambda = \frac{3}{2}\lambda_s\,\cos^2\theta, \tag{7}$$

where θ is the angle between the M_s vectors and the field direction. Recognizing that the bulk magnetization along the field direction is given by $M = M_s\,\cos\theta$, equation (7) becomes

$$\lambda = \frac{3}{2}\lambda_s\left(\frac{M}{M_s}\right)^2, \tag{8}$$

which provides a quadratic relation between the magnetization and magnetostriction. It has been shown that this expression is sufficiently accurate in a broad range of transducer regimes in which high mechanical preloads are employed to optimize transducer performance [24]. A generalized version of this equation has been given in [25], while more elaborate models for magnetostriction hysteresis have been presented in [19, 26, 27, 28]. Additional effects such as stress dependencies have been also considered [25, 29]. Finally, the dependency of the magnetostriction of the R-Fe_2 compounds with temperature has been discussed in [8].

5 Other Magnetostrictive Effects

Joule magnetostriction is one of several manifestations of a more general phenomenon, that is the coupling between the magnetic and elastic regimes in a magnetostrictive material. These effects are briefly discussed below and summarized in Table 3.

5.1 Villari effect

The Villari effect, also known as the magnetomechanical effect, refers to the changes in magnetization that a magnetostrictive material undergoes when subjected to an applied uniaxial stress. This effect pertains to the transduction of energy from the elastic to the magnetic state, and as such is the inverse of the Joule magnetostriction. Furthermore, the Villari effect exhibits many of the attributes of the direct magnetostrictive effect inasmuch as its physical origin also lies in the magnetoelastic coupling. The Villari effect has been the object of much study given its relevance in applications such as nondestructive evaluation and sensing. Extensive theoretical and experimental details can be found in [25]. The effect of stress on magnetostrictive materials in particular has been discussed in [30].

5.2 ΔE effect

The elasticity of magnetostrictive materials is composed of two separate but related attributes, namely the conventional stress-strain elasticity arising from interatomic forces and the magnetoelastic contribution due to the rotation of magnetic moments and ensuing strain which occur when a stress is applied. This is known as the ΔE effect and is quantified by $\Delta E = (E_s - E_0)/E_0$, where E_0 is the minimum elastic modulus and E_s is the elastic modulus at magnetic saturation. Because the strain produced by magnetic moment rotation adds to the non-magnetic strain, the material becomes softer when the moments are free to rotate. This is illustrated in Figure 8. Note that the material becomes increasingly stiffer as saturation is approached and magnetic moment mobility decreases. The ΔE effect is small in nickel ($\Delta E = 0.06$), but is quite large in Terfenol-D (ΔE up to 5) and certain transverse-field annealed $Fe_{81}B_{13.5}Si_{3.5}C_2$ (Metglas 2605SC) amorphous ribbons ($\Delta E = 10$). The ΔE effect of Terfenol-D can be advantageously employed in tunable vibration absorbers and broadband sonar systems [31].

5.3 Wiedemann effect

A current-carrying ferromagnetic or amorphous wire will produce a circular magnetic field in a plane perpendicular to the wire and the moments will align predominantly in the circumferential direction. When an axial magnetic field is applied, some of the moments align in a helical fashion creating a helical magnetic field. The twist observed in the wire is called the Wiedemann effect. The inverse Wiedemann effect, known as the Matteuci effect, is the change in axial magnetization of a current carrying wire when it is twisted. Further details can be found in [2].

5.4 Magnetovolume effect

While the volume of a magnetostrictive material remains virtually unchanged during normal operation, in certain extreme regimes the volume of the material may change in response to magnetic fields. This anomalous volume change is called the volume magnetostriction or Barret effect. The effect has little applicability in smart structure systems. For instance, while the magnetostriction curve of nickel rapidly reaches -35×10^{-6} at only 10 kA/m, the fractional volume change is only 0.1×10^{-6} at a much larger

field of 80 kA/m. In the alloy Invar (36% nickel-64% iron) the fractional volume change at the Curie temperature, which is slightly above room temperature, compensates the intrinsic thermal expansion giving a compound with a nearly zero thermal expansion at room temperature. The inverse of the Barret effect, the Nagaoka-Honda effect, is the change in magnetic state caused by a volume change [14, 2].

6 Magnetostrictive Transducers

One advantage of magnetostrictive transducers over other types of transducers is that they can be driven with conventional low impedance amplifiers, particularly at frequencies well below resonance in which the low impedance of a magnetostrictive transducer means that driving voltages can be low. This can prove useful in medical applications and in general can greatly simplify amplifier design. Figure 9 shows the measured complex electrical impedance frequency response function $Z_{ee} = V/I$ of a Terfenol-D transducer designed following the generic configuration indicated in Figure 10 [32, 33]. This transducer consists of a cylindrical magnetostrictive rod, a surrounding copper-wire solenoid, a preload mechanism consisting of a bolt and spring washer, magnetic couplers and a barrel-like permanent magnet which provides the bias magnetization. While specific design details depend on the particular smart structure application, this configuration depicts the basic components needed to extract maximum performance from the magnetostrictive material.

Because the magnetostriction is produced by the rotation of magnetic moments (see Section 1), a magnetostrictive transducer driven by an AC magnetic field vibrates at twice the drive frequency and the motion takes place in only one direction. This is illustrated in Figure 11, where the solid lines represent the unbiased input and corresponding strain output. The dashed lines demonstrate the performance improvements achieved by applying a magnetic bias to the material. Now the frequency of the input is preserved, the output is bidirectional, and the ratio of output per input is substantially larger. To accurately center operation around the desired bias point, the permanent magnet is often employed in combination with a static field generated by passing a DC current through the solenoid. It is noted that while exclusive permanent magnet biasing has the advantage of substantial power savings, it has the disadvantage of added bulk and weight. Conversely, DC currents produce considerable power losses through ohmic heating but facilitate savings in bulk and weight. The magnetic biasing can be alternatively provided with magnets located in series with the rod or rods, design which is known as stacked-magnet configuration. The stacked-magnet configuration has been observed to provide improvements in the magnetomechanical coupling of up to 5% for large rods ($L > 20$ cm, $D > 2.5$ cm) compared to the barrel-magnet configuration. However, collateral problems such as saturation effects and resonance frequency shifts are common in stacked-magnet designs. Carefully designed transducers must provide efficient magnetic flux closure within the circuit formed by the rod itself, the couplers and the permanent magnets.

Finally, although modern magnetostrictive materials such as Terfenol-D are manufactured with the magnetic moments nearly perpendicular to the rod axis, a static stress (mechanical preload) is nevertheless required for achieving full alignment of all the moments. A mechanically free rod has the moments aligned randomly and will only produce about half of its maximum magnetostriction because the moments initially aligned with the rod axis do not contribute to the magnetostriction. Furthermore, the stress anisotropy generated by the static compression (or tension in the case of materials with negative magnetostriction) will enhance the overall magnetoelastic state of the material in the manner described in Section 3.1. It is emphasized that, in designs which employ linear washers for preloading, the stress in the magnetostrictive rod can vary significantly in relation to the nominal preload during dynamic transducer operation. By virtue of the magnetomechanical coupling, this can have a profound impact on the performance of the magnetostrictive transducer and driving electronics by affecting the magnetic state and, through it, the electrical regime (see Figure 9). The effects of mechanical preload and magnetic bias on the performance of a Terfenol-D transducer have been studied in [34]. A second reason for employing a mechanical preload is to avoid operating the rod in tension, particularly when driving brittle materials such as Terfenol-D ($\sigma_t = 28$ MPa, $\sigma_c = 700$ MPa) at or near mechanical resonance.

6.1 Actuator applications

The number of actuator applications based on magnetostrictive materials, mainly Terfenol-D, is continuously increasing as a consequence of the high energy density, high force, broad frequency bandwidth and fast

response that these materials can provide. Even though the cost of Terfenol-D is high at present, the range of applications will likely continue to increase as manufacturing techniques are perfected and prices decline. Actuators designed according to the configuration shown in Figure 10 have been employed, among others, in the following applications: sonar, chatter control of boring tools, high-precision micropositioning, borehole seismic sources, geological tomography, hydraulic valves for fuel injection systems, deformable mirrors, hydraulic pumps, bone-conduction hearing aids, exoskeletal telemanipulators, self-sensing actuators, degassing in manufacturing processes such as rubber vulcanization, and industrial ultrasonic cleaning. A discussion regarding current transducer designs is presented below in the context of four main applications subgroups: sonar transducers, linear motors, rotational motors and hybrid smart material transducers. The reader is directed to [1, 2] for more complete details.

6.1.1 Sonar transducers

Efficient sonar transducers must produce high mechanical power at low frequencies, often with the additional constraint that a broad frequency bandwidth or equivalently, a low quality factor Q, must be attained. Although nickel was widely employed in sonar applications during the second world war, it features a low magnetomechanical coupling coefficient of $k = 0.30$ which typically demands that Q be high in order for good efficiencies to be achieved. In contrast, the newer giant magnetostrictive materials have a much higher coupling coefficient of over $k = 0.70$ which makes it possible to simultaneously operate the transducer at low Q and attain high power outputs. For example, a Terfenol-D Tonpilz transducer similar to that depicted in Figure 12(a) can produce a bandwidth of 200 Hz at a resonance frequency of 2 kHz ($Q = 10$) and a source level of 200 dB ref. 1 μPa at 1 m [35]. Another Terfenol-D transducer has been reported to produce a maximum output of 206 dB ref. 1 μPa at 1 m, and operate over a broad usable bandwidth of 50 Hz-5 kHz [36]. Other designs employ the linear motion of cylindrical magnetostrictive rods to flex a surrounding shell or to induce radial vibrations in a tube or ring, as shown in Figures 12(b),(c). Further details and references are provided in [37].

6.1.2 Linear motors

The direct coupling between the load and magnetostrictive element in Figure 10 implies that the net load displacement will be limited by the magnetostriction. For instance, a 11.4-cm Terfenol-D actuator will provide maximum displacements of about 0.2 mm. While this kind of displacement is sufficient for many vibration control applications, certain systems such as flow control valves or aircraft flap positioners typically require much larger strokes.

The fact that the Joule magnetostriction takes place at constant volume is employed in the Kiesewetter motor to displace loads beyond the maximum strain normally achievable with a Terfenol-D rod. This motor [38] consists of a cylindrical Terfenol-D rod which fits snugly inside a stiff stator tube when no magnetic field is applied. Several short coils surround the stator so as to produce a magnetic field profile that sweeps along the Terfenol-D rod. When one of the coils is energized, for instance coil No. 1 in Figure 13(a), the section of rod directly exposed to the magnetic field elongates and shrinks. As the field is removed, the rod clamps itself again inside the stator but at a distance d to the left of the original position. As the remaining coils are energized sequentially and the magnetic field profile is swept, the rod moves in the direction opposite to the sweeping field. The direction of motion is changed by inverting the sequence in which the coils are energized. Since a design perspective, the total displacement is limited only by the length of the Terfenol-D rod, whereas the speed of motion is proportional to the sweeping frequency and the magnetostriction of the rod. Other factors affect the smoothness and speed of the motor such as the number of traveling pulses, the spacing between excitation coils, the stiffness of the Terfenol-D material and skin effect degradation due to eddy currents. The Kiesewetter motor is self locking when unpowered, which is an important attribute for many robotic applications.

A proof-of-concept Kiesewetter motor has been presented in [39] which produces 1000 N of force, 200 mm of useful stroke and a speed of 20 mm/s, intended for uses such as control of coat weight and fiber distribution in the paper industry or valve operation and precision positioners for the machine tool industry. An improved design presented in [40] addresses some of the technological issues of the Kiesewetter motor, particularly the degradation of fit between stator and rod caused by wear and thermal expansion. Furthermore, this revised design enables rotary motion in a way which is otherwise impossible to achieve with the original Kiesewetter

design.

Another variant of the inchworm principle is shown in Figure 13(b). This motor consists of translating clamps, fixed clamps, pusher transducers and a load shaft. By coordinating the clamping and unclamping actions of the clamps with the action of the pushing transducers, it is possible to induce bidirectional motion of the load shaft. The load rating is limited by the frictional force between the clamps and the load shaft. It is noted that the inchworm principle can be implemented with other smart materials as well, such as piezoelectric stacks [41], or a combination of piezoelectric and magnetostrictive elements as shown later in Section 6.1.4.

Although piezoelectric transducers are often preferred for ultrasonic power generation in the MHz range, certain applications in the low-ultrasonic range benefit from the ruggedness and lack of depoling mechanisms of magnetostrictive materials. For instance, nickel is being extensively used in applications such as degassing of liquids (20-50 kHz) and cleaning of dental or jewelry pieces (over 50 kHz). A surgical ultrasonic tool based on Terfenol-D has been developed recently which is reported to provide enhanced power and displacement outputs over existing piezoelectric tools, while being lighter, more compact and featuring the ability to deliver a 600 V, 1 MHz signal to cauterize bleeds without interfering with its surgical function. In this device, illustrated in Figure 14, a laminated quarter wavelength Terfenol-D rod is coupled to a quarter wavelength titanium waveguide which provides the resonant subassembly to which a half wavelength acoustic horn is attached. The acoustic horn provides an amplification factor of between 15-30 thus providing extreme accelerations and energy concentration at the tip of the tool [42, 43]. Other current or potential uses for such transducer design include industrial cleaning, sonic cell disruption and sterilization, friction welding, and treatment of diverse chemical and biological processes [1].

6.1.3 Rotational motors

Smart material motors based on the magnetostrictive principle are not only possible but potentially simpler and more reliable than conventional hydraulic or electromagnetic systems. The inchworm technique has been employed in a rotational motor which produces a torque of 3 N.m and a speed of 0.5 rpm [44]. Another device of the inchworm type also provides a speed of 0.5 rpm but produces a very high torque of 12 N.m and precision microsteps of 800 μrad [45]. Despite the great position accuracy and high holding torques, the current inchworm-type rotational motors tend to lack efficiency. Much of the efficiency limitation has been overcome in the resonant rotational motor proposed by Claeyssen et al. [46]. Two linear Terfenol-D actuators are used to induce elliptic vibrations on a circular ring that acts as a stator and which transmits the vibrations to rotational rotors pressed against the ring. The prototype is reported to provide a maximum torque of 2 N.m and a maximum speed of 17 rpm.

Much research and commercial interest is placed on the area of ultrasonic rotational motors. These motors are employed in a wide range of applications from autofocusing camera lenses to robotic manipulators. A rotational actuator has been developed by Akuta [44] which employs Terfenol-D to achieve a relatively high speed of 13.1 rpm and a maximum torque of 0.29 N.m. As depicted in Figure 15, this motor employs two Terfenol-D exciter rods to induce rotations in the shaft.

6.1.4 Hybrid magnetostrictive/piezoelectric devices

Given their technological interest, hybrid smart material actuators can be considered in a separate class independently of whether they are intended for sonar, linear or rotational applications. Because magnetostrictive materials are inductive and piezoelectric elements are capacitive, it is advantageous to combine both types of materials in the same device so that a resonant electric circuit is formed. When driven at resonance, such a device behaves like a purely resistive load and only the energy effectively converted to mechanical motion or lost to inner losses needs to be supplied externally. This greatly simplifies amplifier design and helps for attaining high efficiencies.

To overcome the difficulties involved in achieving motion at only one end of a Tonpilz piston-type sonar transducer, a hybrid device has been demonstrated which consists of a quarter wavelength stack of piezoelectric Navy type I ceramic rings joined to a quarter wavelength Terfenol-D composite tube (see Figure 16(a) and reference [47]). The inherent 90^o phase shift between the magnetostrictive and piezoelectric transduction processes in combination with the quarter wavelength design of the elements ensures addition at one end and cancellation at the other. While the device is *mechanically* unidirectional, it becomes *acoustically*

unidirectional only under array-baffled operation. The measured front-to-back pressure ratio is 5 dB for the device alone and 15 dB under array-loaded conditions. The concept of hybrid piezoelectric/magnetostrictive transduction has been also implemented for linear inchworm motors [48, 49] and rotational motors [50]. For instance, the prototype presented in [48] has a configuration as shown in Figure 13(b), but in which the clamping is done by piezoelectric stacks and the translation is provided by Terfenol-D rods. The intrinsic 90^o phase lag between the two types of elements provides a natural drive timing for the inchworm, while the direction of motion can be easily reversed by changing the magnetic bias on the Terfenol-D elements. This motor achieves a zero-load speed of 25.4 mm/sec and a stall load of 115 N.

A hybrid magnetostrictive/piezoelectric rotational motor is illustrated in Figure 16(b) following the proof-of-concept transducer presented in [50]. A piezoelectric stack clamps a piece of friction material onto the rotating disk, while two magnetostrictive rods move the clamp tangentially to the disk to produce the rotational motion. The sequence of the motion is, as indicated before, determined by the natural timing of the piezoelectric and magnetostrictive response. The device produces a speed of 4 rpm at excitation voltages of between 30-40 V and frequencies of between 650-750 Hz.

6.2 Sensor applications

As evidenced by the growing number of publications and patents, magnetostrictive materials are being employed in a wide variety of sensor designs. In this overview, the term sensor is used in a broad sense to indicate the attributes of magnetostrictive materials which facilitate generation of electrical signals in response to mechanical excitations such as force, strain and torque, or magnetic excitations such as magnetic fields. By virtue of the magnetomechanical coupling, changes in the magnetoelastic state through these parameters (or a combination of them) produces measurable changes in the magnetization anisotropy. To complete the sensing mechanism, a pick-up coil is often wrapped around the magnetostrictive material to detect the magnetization changes, effectively providing a mechanism for conversion from the magnetic to electrical regimes. The principle that links the magnetization in the material with the voltage V generated across a pick-up coil is the Faraday-Lenz law of electromagnetic induction,

$$V = -N\,A\,\frac{dB}{dt},$$

in which N and A are, respectively, the number of turns and constant cross-sectional area of the coil, and B is the magnetic induction which quantifies the magnetization state through $B = \mu_0(H + M)$ [21]. Alternatively, interferometry techniques can be employed to detect the changes in wave speed which occur when the magnetostrictive material changes its properties in the presence of external excitations, for instance the stiffness changes associated with the ΔE effect as described in Section 5.

An overview of sensor designs is presented next, in which emphasis is placed on the main operating principles which enable operation of the sensors. While the list is not comprehensive, it is noted that a huge number of alternative designs can be devised based on the fundamental operation principles presented here. Further details can be found in the provided references.

6.2.1 Torque sensors

Magnetostrictive noncontact torquemeters have been devised based on the principle that the torque applied to a shaft generates stresses of opposite sign $+\tau$ and $-\tau$ oriented at $\pm 45^o$ from the shaft axis. If the shaft is magnetostrictive or has a magnetostrictive amorphous ribbon bonded onto it, the magnetic properties along the directions of $+\tau$ and $-\tau$ will change. These properties can be measured either in a differential fashion with a set of perpendicular coils as shown in Figure 17(a), or through a single Hall effect or similar magnetic field intensity sensor [51]. This kind of sensor can be employed, for instance, in fly-by-wire steering systems for the automotive industry. Additional details and references can be found in [2].

Another class of noncontact torquemeters relies on the changes in permeability exhibited by a magnetostrictive material subjected to torsional stress. In particular, applications requiring less sensitivity can benefit from the elevated mechanical strength that magnetic steels or alloys can provide. One such example is shown in Figure 17(b), in which the working torque on a drill bit is detected with two sensing coils connected in series and located one over the flutes and the other over the shank (the permeability of the shank is less sensitive to changes in torque than the flutes.) An excitation coil provides the AC magnetic

field excitation, while the sensor's proportional output is the differential voltage generated by the sensing coils as the permeability of the bit changes due to the applied torque [52].

6.2.2 Deformation and position sensors

Transverse-field annealed magnetostrictive ribbons or wires make very sensitive strain gauges. A sensor of this kind has been made from strips of Metglas 2605SC transverse annealed for 10 min. in a 208 kA/m (2.6 kOe) magnetic field at 390 °C and rapidly cooled in a saturation field [53]. The sensor responds to the changes in permeability of the ribbon, which by virtue of the magnetomechanical coupling depends in turn on the state of strain in the material. Defining a dimensionless gauge factor as the fractional change in the measured parameter (in this case permeability) by the change in strain, $F = (\partial\mu/\partial S)/\mu$, this sensor has an F equal to about 250,000, which compares extraordinarily well with resistive strain gauges ($F = 2$) and semiconductor gauges ($F = 250$). One problem encountered with this device is that normal thermal expansion can saturate the sensor. This problem can be overcome by bonding the material with a highly viscous liquid, although this limits operation to AC regimes.

A position detector can be accomplished with a magnetostrictive material employed as an acoustic waveguide. Such a device, shown in Figure 18, consists of a permanent magnet which is connected to the target and rides along the length of the waveguide, an emitter/receiver head which sends and receives either an acoustic or current pulse down the waveguide, and a damper which prevents unwanted wave reflections. The principle of operation of the sensor is rather simple: the magnet interacts with the magnetostrictive waveguide and locally changes its material properties. These material property change can be detected in different ways. In one version, the stiffness discontinuity produced by the magnet (ΔE effect) partially reflects back an acoustic pulse sent by the emitter. In a second version, the emitter sends a continuous current pulse down the waveguide which produces a circumferential magnetic field that interacts with the axial field from the magnet. The resulting helical field produces a twist in the wire (Wiedemann effect) which travels back to the receiver head. In both versions, the transit times of the original and reflected pulses provide a measure of the location of the magnet along the waveguide. This sensor can be used to measure fluid levels by connecting the magnet to a float or for generic position sensing of up to 50 m with ±1 mm accuracy [2].

6.2.3 Magnetometers

If the magnetostriction of a given material is known as a function of magnetic field, the problem of measuring magnetic field reduces into one of measuring length. The length can be measured with a laser interferometer, optic fiber, strain gauge, capacitor or with another calibrated material such as a piezoelectric compound. For example, a very simple design consists of two slabs of magnetostrictive and piezoelectric materials bonded together (Figure 19(a)). When a magnetic field is applied to the magnetostrictive material, it strains, thus inducing a proportional voltage in the piezoelectric material. In another version, shown in Figure 19(b), a magnetometer is realized by bonding a field-annealed metallic glass ribbon onto a resonating PZT plate with a viscous fluid. An alternating voltage is applied to the PZT plate, which generates a longitudinal stress field. With proper bonding techniques, the dynamic stress in the metallic ribbon is congruent with that in the PZT while the static component is filtered out by the viscous fluid. By virtue of the Villari effect, these dynamic stresses create an oscillating electromotive force (e.m.f.) in the surrounding pick-up coil. When exposed to low-frequency magnetic fields, a low-frequency e.m.f. is generated in the coil which is extracted from the carrier e.m.f. with conventional phase sensitive detection techniques. The measured detection limit can reach 6.9×10^{-6} A/m at 1 Hz [54], which compares with that of fluxgate magnetometers.

Another type of magnetometer consists of a magnetostrictive film coating bonded onto an optic fiber. When the sensor is exposed to magnetic fields, the magnetostrictive material deforms and so does the optic fiber. This causes changes in the optical path length of laser beams passing through the optic fiber, which can be detected by an interferometer [55]. Highly sensitive metallic glass ribbons have been employed in devices so designed, yielding quasistatic resolutions of between 1.6×10^{-3}-8.0×10^{-3} A/m [56]. Finally, a diode laser interferometer has been used to detect changes in length of a Terfenol-D rod produced when a magnetic field is applied [57]. A maximum sensitivity of 160×10^{-6} A/m was achieved, although certain nonlinear dependencies were observed which make it critical to operate the sensor within its optimum mechanical preload range.

6.2.4 Force sensors

Employing the Villari effect, it is possible to realize a simple and rugged force sensor employing either crystal or amorphous magnetostrictive materials. The magnetostrictive attribute which provides the operating principle for such a sensor is the dependency of the magnetization with the state of stress in the material. To illustrate, the design in Figure 20 consists of two magnetostrictive elements, one surrounded by an excitation coil and the other surrounded by a pick-up coil, and two rigid end plates. In one mode of operation, an AC voltage is applied to the excitation coil which generates a magnetic flux in the sensor and a corresponding voltage in the sensing coil. As a force is applied, the magnetostriction in the elements produces a change in the magnetic flux which is detected as a proportional voltage change in the pick-up coil. In a second mode of operation at constant flux, the excitation voltage is allowed to change in order to maintain a constant pick-up coil output voltage. The change in excitation voltage is then related to the change in applied force. Compared to conventional force sensors such as those based on strain gauges, this sensor is simpler, more rugged and requires simpler electronics. A similar Villari effect sensor based on amorphous ribbons has been discussed in [58]. Numerous other designs have been discussed or patented, including percussion sensors, pressure sensors and force sensors based on magnetoelastic strain gauges. The reader is directed to [2] for further details and references.

7 Concluding Remarks

The magnetomechanical coupling present in magnetostrictive materials provides a robust mechanism for bidirectional conversion of energy between the magnetic and elastic states. In addition, newer materials such as Terfenol-D or amorphous metallic ribbons provide a unique combination of high forces, strains, energy densities, operating bandwidths and coupling coefficients which has justified their use in an ever-increasing number of actuators and sensor applications ranging from micropositioning to vibration control of heavy machinery. The excellent performance of magnetostrictive materials is sometimes obscured by the hysteresis and nonlinear effects which are intrinsic to magnetostriction. In this sense, achievement of full performance with magnetostrictive materials poses rigorous engineering challenges in a way which other less capable smart materials do not. However, as evidenced by the increasing number of patented devices based on magnetostrictive principles, transducer designers continue to overcome these challenges and make advances in design, modeling and control of magnetostrictive device performance attributes. Furthermore, clever transducer designs are possible solely due to the rich performance space which arises as a consequence of the otherwise undesirable nonlinear characteristics of these materials. As material advances continue, it is expected that magnetostrictive device designers will find new magnetostrictive solutions to an ever-growing variety of transducer applications.

Table 1: Magnetoelastic properties of some magnetostrictive materials. Unless otherwise specified, all measurements where performed at room temperature.

Material	$\frac{3}{2}\lambda_s(\times 10^{-6})$	ρ (g/cm^3)	B_s (T)	T_c (°C)	E (GPa)	k
Fe	-14 [8]	7.88 [14]	2.15 [14]	770 [14]	285 [14]	
Ni	-50 [14]	8.9 [14]	0.61 [14]	358 [14]	210 [1]	0.31 [8]
Co	-93 [14]	8.9 [14]	1.79 [14]	1120 [14]	210 [1]	
50%Co–50%Fe	87 [2]	8.25 [8]	2.45 [75]	500 [14]		0.35 [8]
50%Ni–50%Fe	19 [2]		1.60 [75]	500 [14]		
$TbFe_2$	2630 [8]	9.1 [14]	1.1 [2]	423 [8]		0.35 [8]
Tb	3000 (−196°C) [36]	8.33 [14]		-48 [13]	55.7 [1]	
Dy	6000 (−196°C) [36]	8.56 [14]		-184 [1]	61.4 [1]	
Terfenol-D	1620 [8]	9.25	1.0	380 [75]	110 [76]	0.77 [77]
$Tb_{0.6}Dy_{0.4}$	6000 (−196°C) [36]					
Metglas 2605SC	60 [36]	7.32 [2]	1.65 [75]	370 [2]	25-200 [2]	0.92 [1]

Table 2: Magnetostriction coefficients of cubic crystal materials.

Material	$\lambda_{100}\,(10^{-6})$	$\lambda_{111}\,(10^{-6})$
Nickel	-46	-24
Iron	21	-21
Terfenol-D	90	1600

Table 3: Magnetostrictive effects.

Direct Effects	Inverse Effects
Joule magnetostriction Change in sample dimensions in the direction of the applied field	**Villari effect** Change in magnetization due to applied stress
ΔE effect Magnetoelastic contribution to magnetocrystalline anisotropy	Magnetically induced changes in the elasticity
Wiedemann effect Torque induced by helical anisotropy	**Matteuci effect** Helical anisotropy and e.m.f. induced by a torque
Magnetovolume effect Volume change due to magnetization (most evident near the Curie temperature)	**Nagaoka-Honda effect** Change in the magnetic state due to a change in the volume

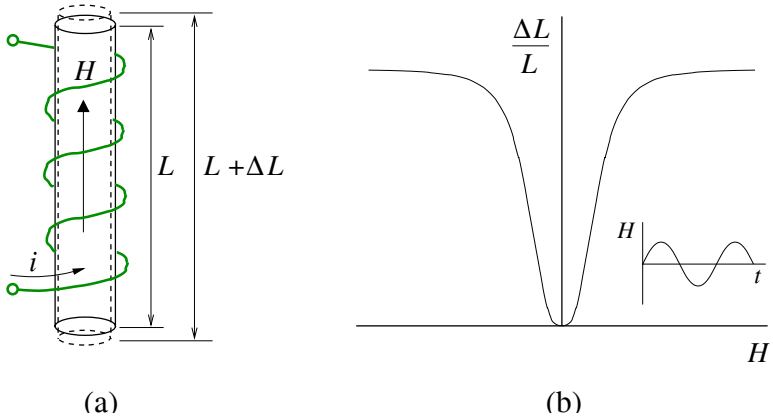

Figure 1: Joule magnetostriction produced by a magnetic field H. (a) H is approximately proportional to the current i that passes through the solenoid when a voltage is applied to it, and (b) curve $\Delta L/L$ vs. H obtained by varying the field sinusoidally (inset).

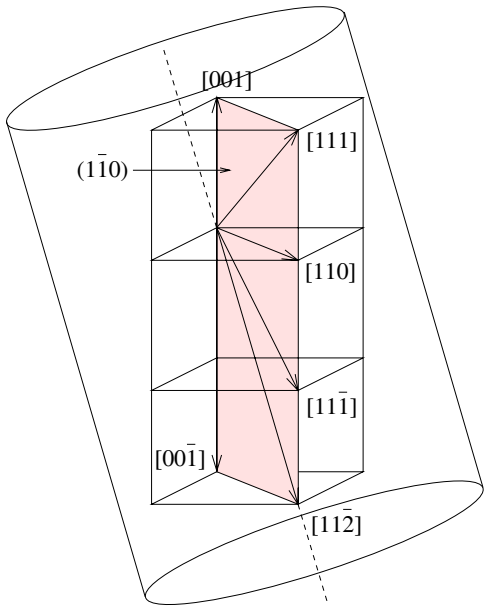

Figure 2: Crystallographic orientations in monolithic Terfenol-D. The square brackets represent the indices of particular directions such as the edges of a cube: [100], [010], [001], [$\overline{1}$00], [0$\overline{1}$0] and [00$\overline{1}$], in which $\overline{1}$ denotes -1. The entire set of directions is designated by any one direction in angular brackets, for instance <100>. Finally, planes of a form are designated by rounded brackets, such as the six faces of a cube: (100), (010), (001), ($\overline{1}$00), (0$\overline{1}$0) and (00$\overline{1}$).

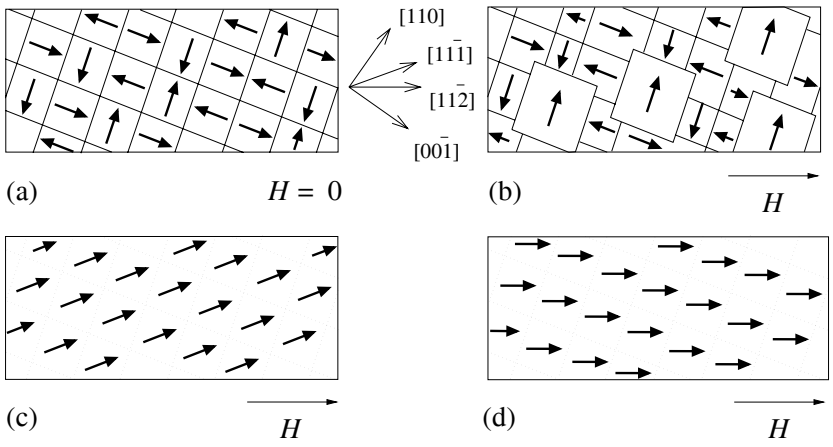

Figure 3: Domain processes in the $(1\bar{1}0)$ plane of single crystal Terfenol-D under the application of a field H along the $[11\bar{2}]$ axis. (a) demagnetized specimen, (b) partial magnetization by domain-wall movement, (c) from partial magnetization to the knee of the magnetization curve by irreversible domain magnetization rotation into the $[11\bar{1}]$ axis and (d) from the knee of the magnetization curve to technical saturation by reversible (coherent) rotation into the $[11\bar{2}]$ axis [21].

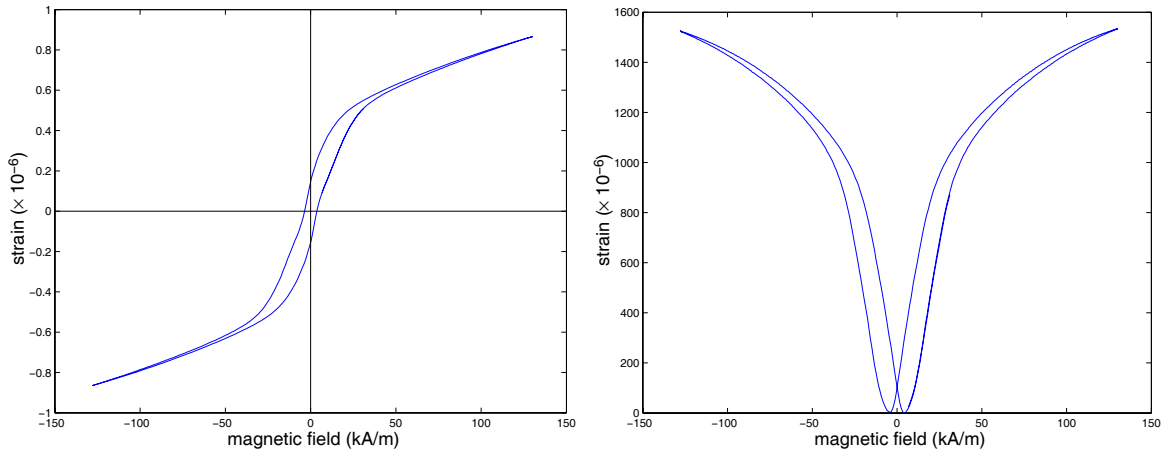

Figure 4: Experimental magnetic induction and total strain, from Terfenol-D loaded at 6.9 MPa.

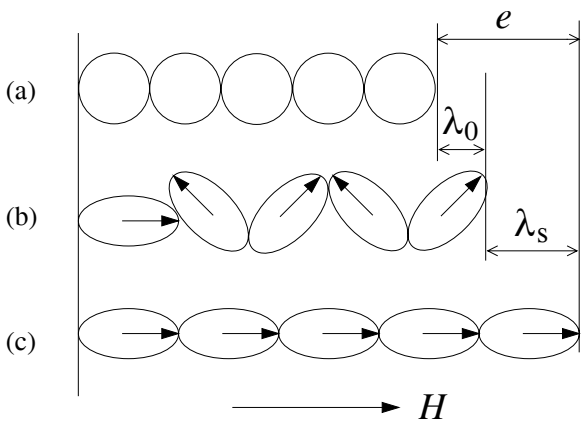

Figure 5: Schematic diagram illustrating the magnetostriction of a ferromagnetic material. (a) paramagnetic state above T_c; (b) after it has been cooled through T_c; and (c) after it has been brought to saturation by a field H.

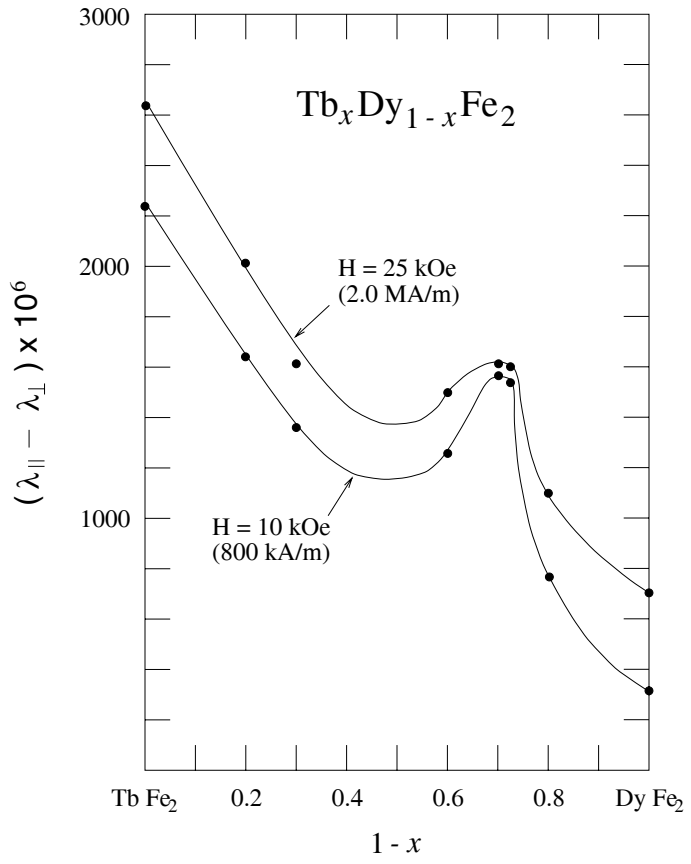

Figure 6: Magnetostriction of polycrystalline $Tb_xDy_{1-x}Fe_2$ at room temperature [8].

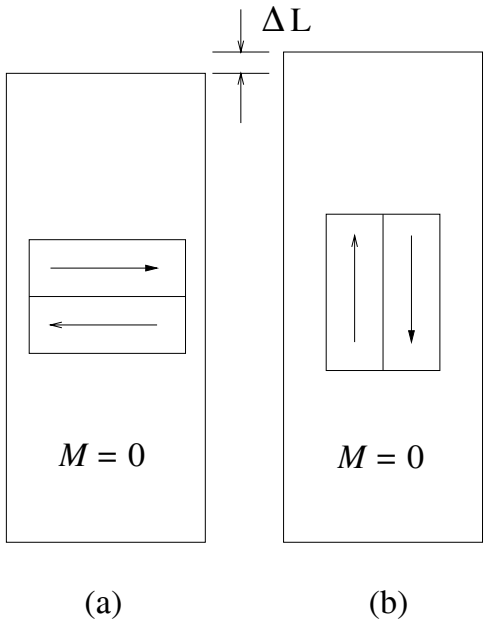

Figure 7: Demagnetized specimen featuring a 180° domain wall in the (a) horizontal or (b) vertical direction. The length of the specimen is different in either case even though the magnetization is the same.

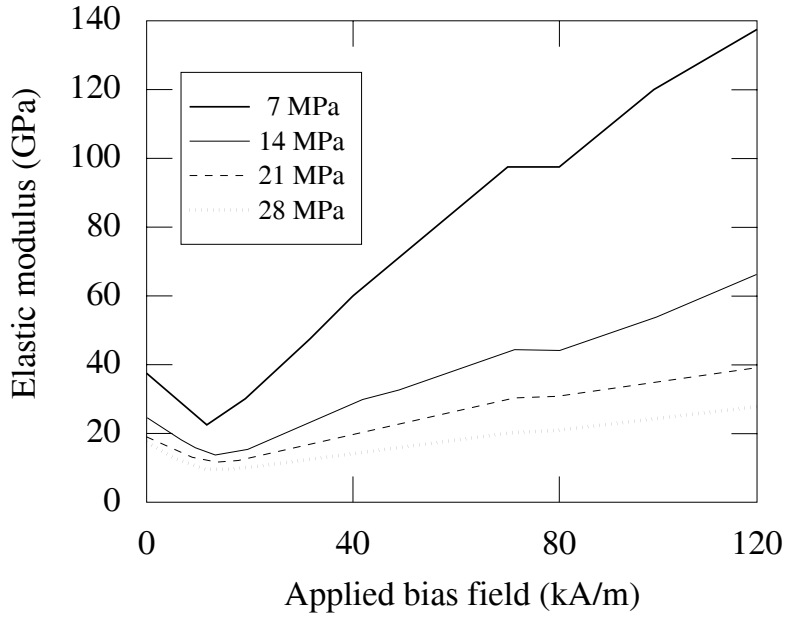

Figure 8: Magnetoelastic modulus of $Tb_{.3}Dy_{.7}Fe_2$ at various stresses [78].

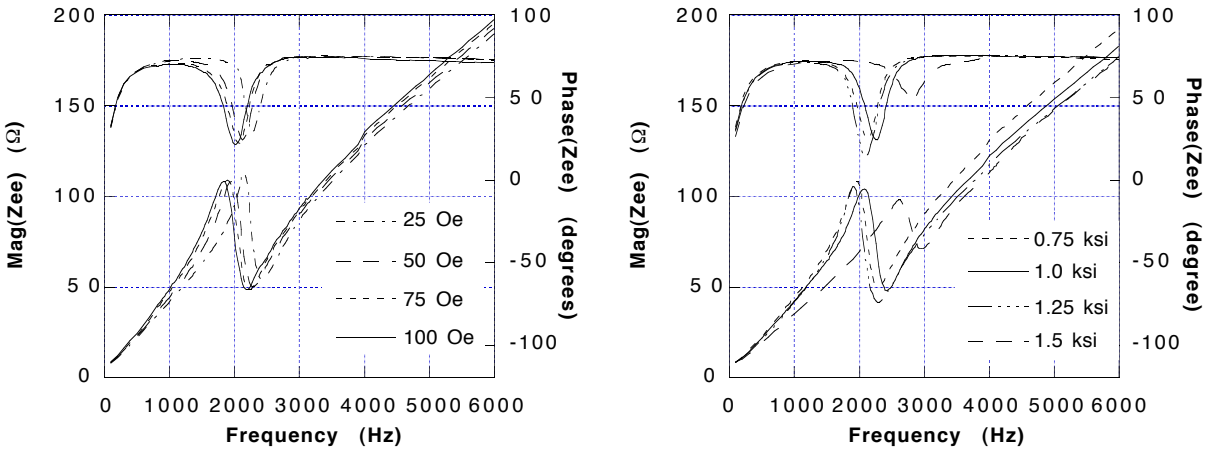

(a) (b)

Figure 9: Total electrical impedance Z_{ee} versus frequency, expressed as magnitude and phase. (a) Bias condition of 5.2 MPa, 24 kA/m (0.75 ksi, 300 Oe) and varied AC drive levels; (b) constant AC drive level of 8 kA/m (100 Oe) and varied bias conditions [78].

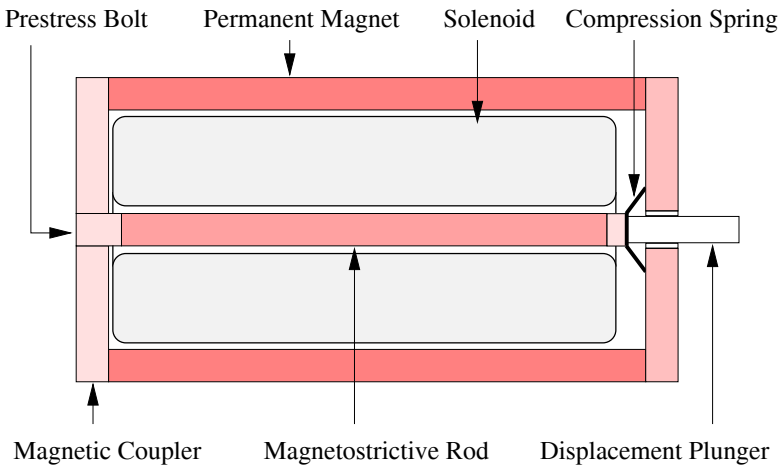

Figure 10: Cross section of a typical magnetostrictive transducer.

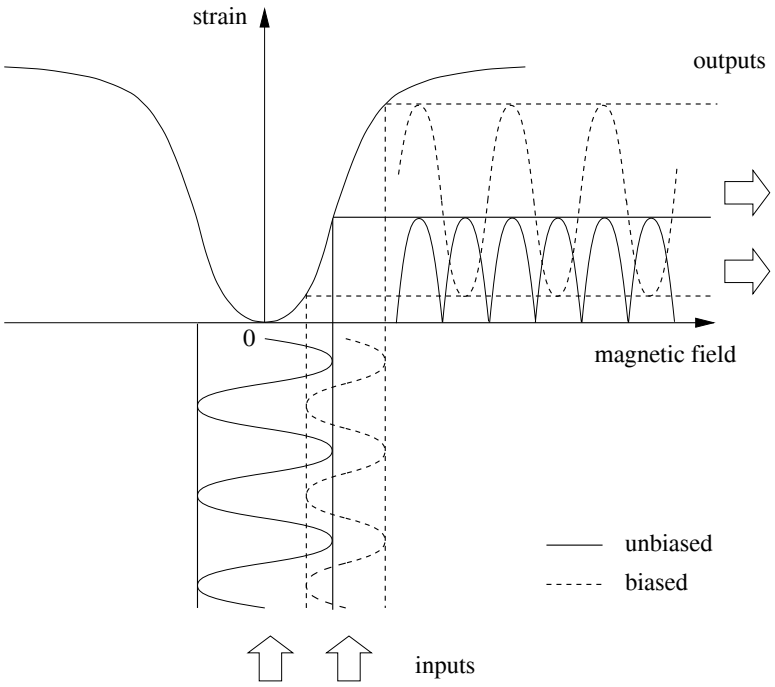

Figure 11: Effect of magnetic bias on the strain produced by a magnetostrictive transducer.

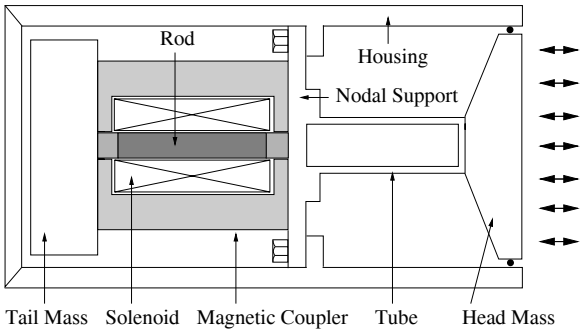

(a)

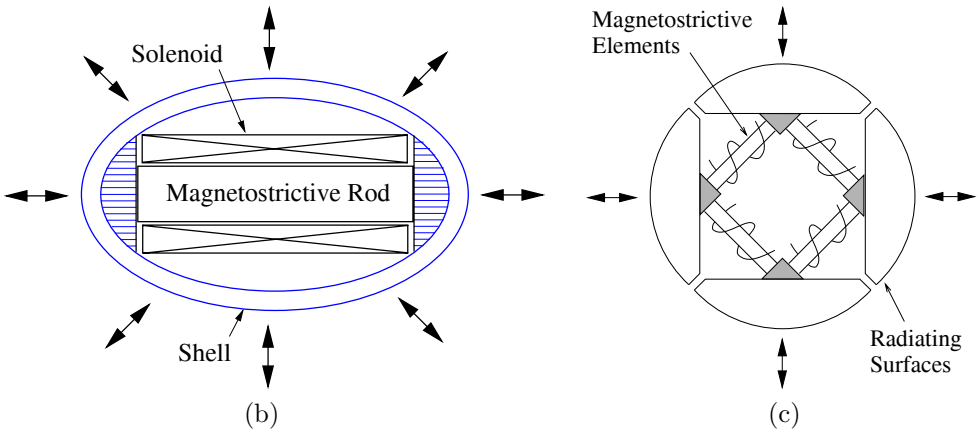

(b) (c)

Figure 12: Magnetostrictive sonar transducers: (a) Tonpilz, (b) flextensional and (c) square ring.

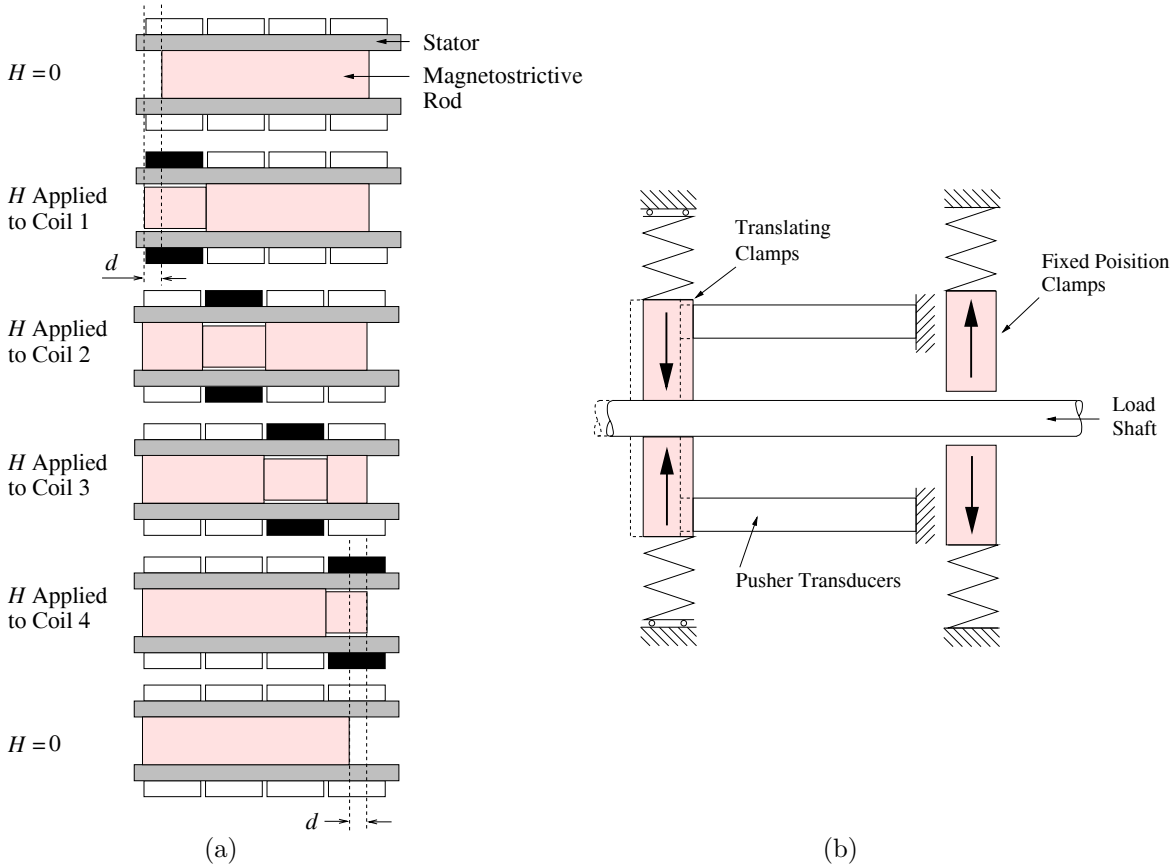

Figure 13: (a) The Kiesewetter inchworm motor. Black rectangles indicate energized coils; white rectangles indicate inactive coils. (b) Inchworm linear motor.

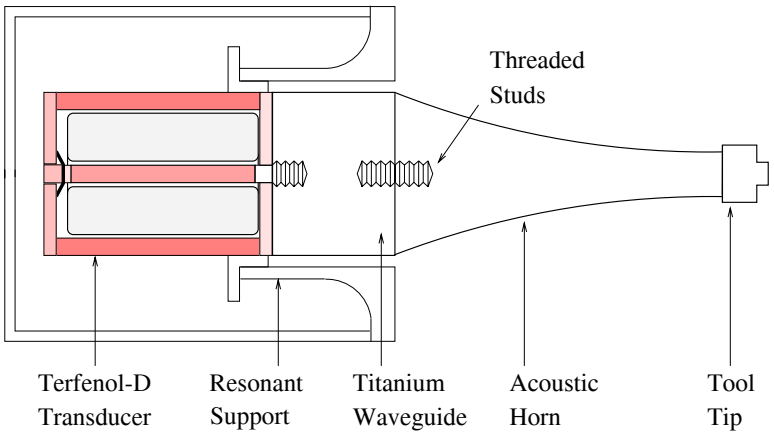

Figure 14: Schematic diagram of an ultrasonic Terfenol-D device consisting of a quarter-wave transducer coupled to a quarter-wave titanium waveguide and a half-wave acoustic horn. Different tool tips can be used as required.

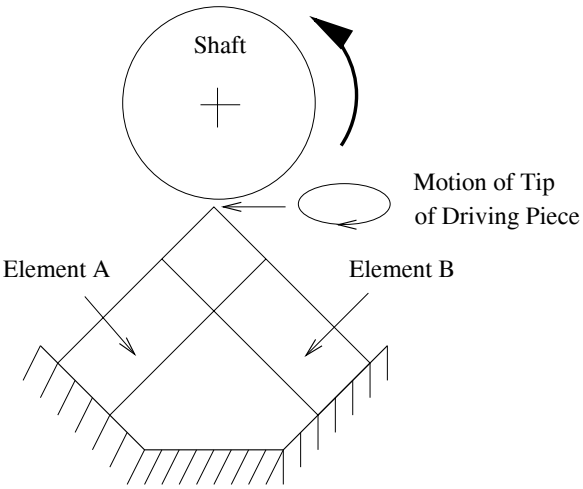

Figure 15: Rotational ultrasonic motor [44].

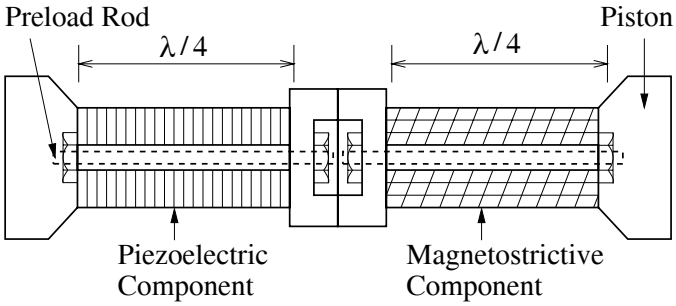

(a)

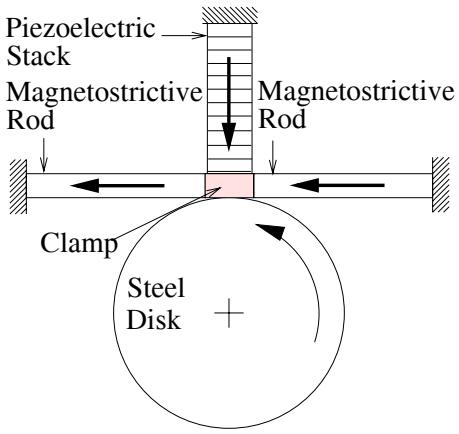

(b)

Figure 16: Hybrid magnetostrictive/piezoelectric transducers. (a) Sonar projector [47], (b) rotational motor [50].

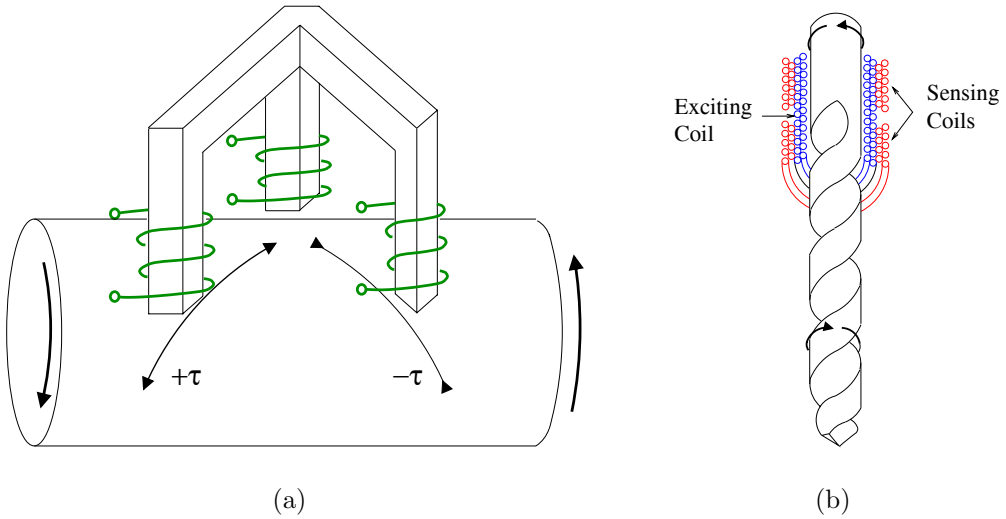

Figure 17: Magnetostrictive noncontact torque sensors. (a) Differential reading along directions oriented $\pm 45^{o}$ from the shaft axis, and (b) differential reading of the permeability changes experienced by a drill bit subjected to a torque.

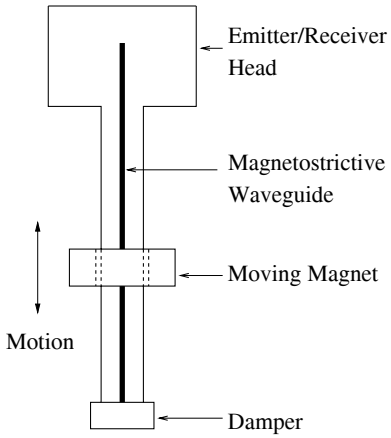

Figure 18: Magnetostrictive waveguide position sensor.

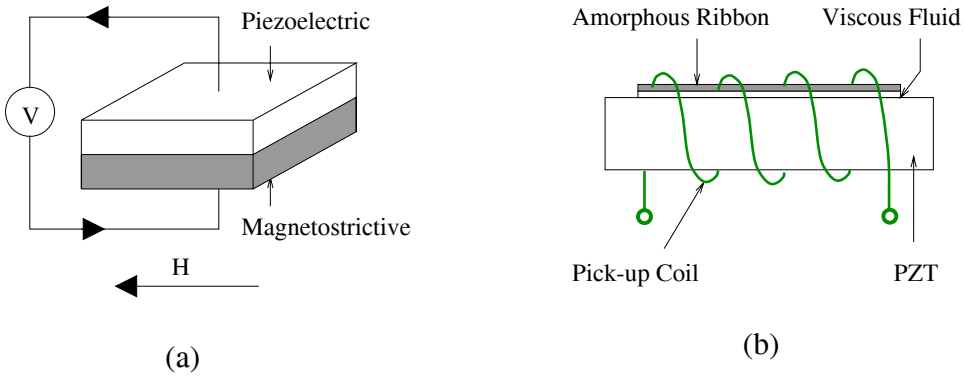

Figure 19: Hybrid magnetostrictive/piezoelectric magnetic field sensors. When a magnetic field is applied to one of these sensors, the magnetostrictive material strains, which either (a) generates a voltage across the piezoelectric plate or (b) induces an e.m.f. in a surrounding pick-up coil which can be extracted from an alternating carrier e.m.f. produced as the piezoelectric plate resonates.

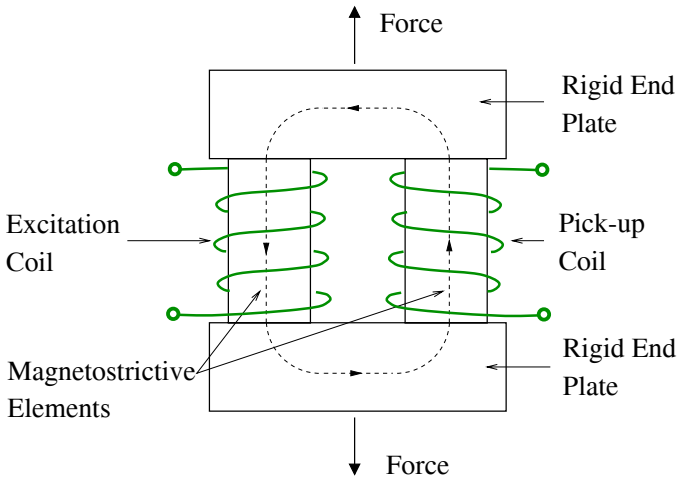

Figure 20: Magnetostrictive force sensor based on the Villari effect.

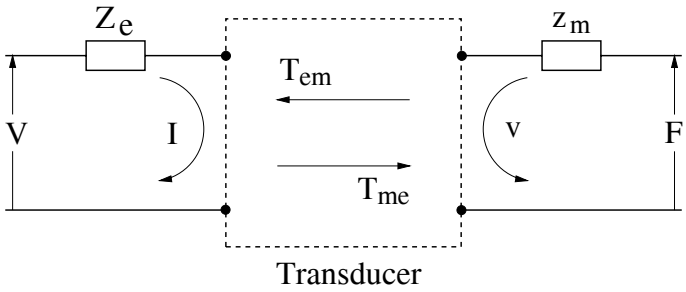

Figure 21: Schematic representation of an electromechanical transducer.

References

[1] G. Engdahl (Ed.). *Handbook of giant magnetostrictive materials*. Academic Press, San Diego, CA, 2000.

[2] E. du Trémolet de Lacheisserie. *Magnetostriction theory and applications of magnetoelasticity*. CRC Press, Inc., Boca Raton, FL, 1993.

[3] T. Cedell. *Magnetostrictive materials and selected applications, Magnetoelastically induced vibrations in manufacturing processes*. PhD thesis, Lund University, Lund, Sweden, 1995. LUTMDN/(TMMV-1021)/1-222/(1995).

[4] T. A. Duenas, L. Hsu and G. P. Carman. Magnetostrictive composite material systems analytical/experimental. In *Adv. Smart Materials Fundamentals and Applications*, Boston, MA, 1996.

[5] M. Anjanappa and Y. Wu. Magnetostrictive particulate actuators: configuration, modeling and characterization. *Smart Mater. Struct.*, **6**:393–402, 1997.

[6] H. Uchida, M. Wada, A. Ichikawa, Y. Matsumara and H.H. Uchida. Effects of the preparation method and condition on the magnetic and giant magnetostrictive properties of (Tb,Dy)Fe_2 thin films. In *Proc. Actuator 96, 5th Intern. Conf. on New Actuators*, pp. 275–278, Bremen, Germany. VDI-VDE, 1996.

[7] C. Body, G. Reyne and G. Meunier. Nonlinear finite element modelling of magneto-mechanical phenomenon in giant magnetostrictive thin films. *IEEE Trans. Magn.*, **33**(2):1620–1623, March 1997.

[8] A. E. Clark. In *Ferromagnetic materials*, Vol. 1, Ch. 7, pp. 531–589. Ed. E. P. Wohlfarth, North Holland Publishing, Co., Amsterdam, 1980.

[9] E.A. Lindgren, J.C. Poret, J.J Whalen, L.P. Martin, M. Rosen, M. Wun-Fogle, J.B. Restorff, A.E. Clark and J.F. Lindberg. Development of Terfenol-D transducer material. In *U.S. Navy Workshop on Acoustic Transduction Materials and Devices*, State College, PA, 13-15 April 1999.

[10] J.B. Restorff, M. Wun-Fogle and A.E. Clark. Temperature and stress dependence of the magnetostriction in ternary and quaternary Terfenol alloys. In *U.S. Navy Workshop on Acoustic Transduction Materials and Devices*, State College, PA, 13-15 April 1999.

[11] R. Tickle, R.D. James, T. Shield, M. Wuttig and V.V. Kokorin. Ferromagnetic shape memory in the NiMnGa system. *IEEE Trans. Magn.*, **35**(5):4301–4310, September 1999.

[12] R.C. O'Handley. Model for strain and magnetization in magnetic shape-memory alloys. *J. Appl. Phys.*, **83**(6):3263–3270, March 1998.

[13] B.D. Cullity. *Introduction to magnetic materials*. Addison-Wesley, Reading, MA, 1972.

[14] R.M. Bozorth. *Ferromagnetism*. D. Van Nostrand, Inc., 1968.

[15] C. Kittel. Physical theory of ferromagnetic domains. *Rev. Mod. Phys.*, **21**:541–583, 1949.

[16] E.W. Lee. Magnetostriction and magnetomechanical effects. *Reports on Prog. in Phys.*, **18**:184–220, 1955.

[17] J.P. Teter, A.E. Clark and O.D. McMasters. Anisotropic magnetostriction in $Tb_{0.27}Dy_{0.73}Fe_{1.95}$. *J. Appl. Phys.*, **61**:3787–3789, 1987.

[18] E.C. Stoner and E.P. Wohlfarth. A mechanism of magnetic hysteresis in heterogeneous alloys. *Phil. Trans. Roy. Soc.*, **A240**:599–642, 1948.

[19] A.E. Clark, H.T. Savage and M.L. Spano. Effect of stress on the magnetostriction and magnetization of single crystal $Tb_{0.27}Dy_{0.73}Fe_2$. *IEEE Trans. Magn.*, **MAG-20**(5), 1984.

[20] D.C. Jiles and J.B. Thoelke. Theoretical modelling of the effects of anisotropy and stress on the magnetization and magnetostriction of $Tb_{0.3}Dy_{0.7}Fe_2$. *J. Magn. Magn. Mater.*, **134**:143–160, 1994.

[21] D.C. Jiles. *Introduction to Magnetism and Magnetic Materials*. Chapman & Hall, London, Second edition, 1998.

[22] S. Chikazumi. *Physics of magnetism*. R. E. Krieger Publishing, Malabar, FL, 1984.

[23] M.J. Dapino, A.B. Flatau and F.T. Calkins. Statistical analysis of Terfenol-D material properties. In *Proc. of SPIE Smart Structures and Materials 1997*, Vol. **3041**, pp. 256–267, San Diego, CA, March 1997.

[24] F.T. Calkins, R.C. Smith and A.B. Flatau. An energy-based hysteresis model for magnetostrictive transducers. *IEEE Trans. Magn.*, **36**(2):429–439, April 2000.

[25] D.C. Jiles. Theory of the magnetomechanical effect. *J. Phys. D: Appl. Phys.*, **28**:1537–1546, 1995.

[26] M.J. Sablik and D.C. Jiles. A model for hysteresis in magnetostriction. *J. Appl. Phys.*, **64**(10):5402–5404, 1988.

[27] M.J. Sablik and D.C. Jiles. Coupled magnetoelastic theory of magnetic and magnetostrictive hysteresis. *IEEE Trans. Magn.*, **29**(3), 1993.

[28] R.D. James and D. Kinderlehrer. Theory of magnetostriction with applications to $Tb_xDy_{1-x}Fe_2$. *Philosophical Magazine B*, **68**(2):237–274, 1993.

[29] V. Agayan. Thermodynamic model for ideal magnetostriction. *Physica Scripta*, **54**:514–521, 1996.

[30] M.J. Dapino, R.C. Smith, L.E. Faidley and A.B. Flatau. A coupled structural-magnetic strain and stress model for magnetostrictive transducers. *J. of Intell. Mater. Syst. and Struct.*, in press, and CRSC Technical Report CRSC-TR99-24.

[31] A.B. Flatau, M.J. Dapino and F.T. Calkins. High-bandwidth tunability in a smart passive vibration absorber. In *Proc. of SPIE Smart Structures and Materials*, Vol. **3327**, pp. 463–473, San Diego, CA, March 1998.

[32] F.T. Calkins and A.B. Flatau. Transducer based measurements of Terfenol-D material properties. In *Proc. of SPIE Smart Structures and Materials 1996*, Vol. **2717**, pp. 709–719, San Diego, CA, March 1996.

[33] A.B. Flatau, F. Pascual, M.J. Dapino and F.T. Calkins. Material characterization of ETREMA Terfenol-D, final report. CATD-IPIRT Contract #95-05, October 1996.

[34] F.T. Calkins, M.J. Dapino and A.B. Flatau. Effect of prestress on the dynamic performance of a Terfenol-D transducer. In *Proc. of SPIE Smart Structures and Materials 1997*, Vol. **3041**, pp. 293–304, 1997.

[35] G.A. Steel. A 2-khz magnetostrictive transducer. In *Transducers for Sonics and Ultrasonics*, pp. 250–258, Lancaster, PA. Technomic, Inc., 1993.

[36] J.B. Restorff. Magnetostrictive materials and devices. In *Encyclopedia of Applied Physics*, Vol. **9**, pp. 229–244. VCH Publishers, Inc., 1994.

[37] M.J. Dapino, F.T. Calkins and A.B. Flatau. Magnetostrictive devices. In *22nd. Encyclopedia of Electrical and Electronics Engineering*, Vol. **12**, pp. 278–305. Ed. J.G. Webster, John Wiley & Sons, Inc., 1999.

[38] L. Kiesewetter. The application of Terfenol in linear motors. In *Proc. 2nd. Inter. Conf. Giant Magnetostrictive Alloys*, Marbella, Spain, October 12-14 1988.

[39] R.C. Roth. The elastic wave motor-a versatile Terfenol driven, linear actuator with high force and great precision. In *Proc. 3rd Int. Conf. New Actuators*, pp. 138–141, Bremen, Germany. AXON Tech., 1992.

[40] J.H. Goldie, M.J. Gerver, J. Kiley and J.R. Swenbeck. Observations and theory of Terfenol-D inchworm motors. In *Proc. of SPIE Smart Structures and Materials 1998*, Vol. **3329**, pp. 780–785, San Diego, CA, March 1998.

[41] W. Chen J. Frank, G.H. Koopmann and G.A. Lesieutre. Design and performance of a high force piezoelectric inchworm motor. In *Proc. of SPIE Smart Structures and Materials 1999*, Newport Beach, CA, March 1999.

[42] T.T. Hansen. Magnetostrictive materials and ultrasonics. Technical report, Chemtech, Dec. 1996. pp. 56-59.

[43] J.R. Frederick. *Ultrasonic Engineering*. Wiley, New York, 1965.

[44] T. Akuta. Rotational type actuators with Terfenol-D rods. In *Proc. 3rd. Int. Conf. New Actuators*, pp. 244–248, Bremen, Germany. VDI-VDE, 1992.

[45] J.M. Vranish, D.P. Naik, J.B. Restorff and J.P. Teter. Magnetostrictive direct drive rotary motor development. *IEEE Trans. Magn.*, **27**:5355–5357, 1991.

[46] F. Claeyssen, N. Lhermet and R.L. Letty. Design and construction of a resonant magnetostrictive motor. *IEEE Trans. Magn.*, **32**(5):4749–4751, 1996.

[47] J.L. Butler, S.C. Butler and A.L. Butler. Hybrid magnetostrictive/piezoelectric tonpilz transducer. *J. Acoust. Soc. Am.*, **94**:636–641, 1993.

[48] J.E. Miesner and J.P. Teter. Piezoelectric/magnetostrictive resonant inchworm motor. In *Proc. of SPIE Smart Structures and Materials 1994*, Vol. **2190**, pp. 520–527, Orlando, FL, 1994.

[49] B. Clephas and H. Janocha. New linear motor with hybrid actuator. In *Proc. of SPIE Smart Structures and Materials 1997*, Vol. **3041**, pp. 316–327, San Diego, CA, March 1997.

[50] R. Venkataraman, W.P. Dayawansa and P.S. Krishnaprasad. The hybrid motor prototype: design details and demonstration results. Technical report, CDCSS, University of Maryland, College Park, MD, 1998. CDCSS T.R. 98-2.

[51] I.J. Garshelis. A torque transducer utilizing a circularly polarized ring. *IEEE Trans. Magn.*, **28**(5):2202–2204, September 1992.

[52] I. Sasada, N. Suzuki, T. Sasaoka and K. Toda. In-process detection of torque on a drill using the magnetostrictive effect. *IEEE Trans. Magn.*, **30**(6):4632–4635, November 1994.

[53] M. Wun-Fogle, H.T. Savage and M.L. Spano. Enhancement of magnetostrictive effects for sensor applications. *J. Mater. Eng.*, **11**(1):103–107, 1989.

[54] M.D. Mermelstein and A. Dandridge. Low-frequency magnetic field detection with a magnetostrictive amorphous metal ribbon. *Appl. Phys. Lett.*, **51**(7):545–547, 1987.

[55] A. Yariv and H. Windsor. Proposal for detection of magnetic field through magnetostrictive perturbation of optical fibers. *Opt. Lett.*, **5**:87, 1980.

[56] A. Dandridge K.P. Koo, F. Bucjolts and A.B. Tveten. Stability of a fiber-optic magnetometer. *IEEE Trans. Magn.*, **MAG-22**:141, 1986.

[57] R. Chung, R. Weber and D. C. Jiles. A Terfenol based magnetostrictive diode laser magnetometer. *IEEE Trans. Magn.*, **27**(6):5358–5360, 1991.

[58] J. Seekercher and B. Hoffmann. New magnetoelastic force sensor using amorphous alloys. *Sensors Actuators*, **A21-A23**:401–405, 1990.

[59] D.A. Berlincourt, D.R. Curran and H. Jaffe. Piezoelectric piezomagnetic materials and their function in transducers. In *Physical Acoustics, Principles and Methods*, Vol. **1**, Part A. Ed. W.P. Mason. Academic Press, New York, 1964.

[60] F.V. Hunt. *Electroacoustics: the analysis of transduction and its historical background*. American Institute of Physics for the Acoustical Society of America, 1982.

[61] D.L. Hall. *Dynamics and vibrations of magnetostrictive transducers*. PhD dissertation, Iowa State University, Ames, Iowa, 1994.

[62] W.F. Brown. *Magnetoelastic interactions*. Springer-Verlag, Berlin, 1966.

[63] I.D. Mayergoyz. *Mathematical models of hysteresis*. Springer-Verlag, New York, 1991.

[64] J.B. Restorff, H.T. Savage, A.E. Clark and M.Wun-Fogle. Preisach modeling of hysteresis in Terfenol-D. *J. Appl. Phys.*, **67**((9)):5016–8, 1990.

[65] A. Reimers and E. Della Torre. Fast Preisach based model for Terfenol-D. *IEEE Trans. Magn.*, **35**:1239–1242, May 1999.

[66] R.C. Smith. Hysteresis modeling in magnetostrictive materials via Preisach operators. *J. Mathematical Systems, Estimation and Control*, **8**(2):249–252, 1998.

[67] E.W. Lee and J.E. Bishop. Magnetic behaviour of single-domain particles. *Proc. Phys. Soc.*, **89**:661, 1966. London.

[68] D.C. Jiles and D.L. Atherton. Theory of ferromagnetic hysteresis. *J. Magn. Magn. Mater.*, **61**:48–60, 1986.

[69] M.J. Dapino, R.C. Smith and A.B. Flatau. Structural-magnetic strain model for magnetostrictive transducers. *IEEE Trans. Magn.*, **36**(3):545–556, 2000.

[70] R.C. Smith and Z. Ounaies. A domain wall model for hysteresis in piezoelectric materials. *CRSC Technical Report CRSC-TR99-33 and J. of Intell. Mater. Syst. and Struct.*, in press, 2000.

[71] R.C. Smith. Smart structures: model development and control applications. In *Series on Applied and Computational Control, Signals and Circuits (ACCSC)*. Ed. Biswa Datta. Birkhauser. in press.

[72] R.C. Smith and R.L. Zrostlik. Inverse compensation for ferromagnetic hysteresis. In *Proc. 1999 IEEE Conf. on Decision and Control*, Phoenix, AZ, December 7-10 1999.

[73] M.J. Dapino, F.T. Calkins, R.C. Smith and A.B. Flatau. A magnetoelastic model for magnetostrictive sensors. In *Proceedings of ACTIVE 99*, Vol. **2**, pp. 1193–1204. Ed. Scott Douglas. INCE USA, December 02-04 1999.

[74] R.C. Smith M.J. Dapino and A.B. Flatau. A model for the ΔE effect in magnetostrictive transducers. In *Proc. SPIE Smart Structures and Materials 2000*, Vol. **3985**, pp. 174–185, Newport Beach, CA, 6-9 March 2000.

[75] D.C. Jiles. *Introduction to the electronic properties of materials*. Chapman & Hall, London, 1994.

[76] R.A. Kellogg and A.B. Flatau. Blocked force investigation of a Terfenol-D transducer. In *Proc. of SPIE Smart Structures and Materials 1999*, Vol. **3668**, Newport Beach, CA, March 1999.

[77] A.E. Clark, J.P. Teter, M. Wun-Fogle, M. Moffett and J. Lindberg. Magnetomechanical coupling in Bridgman-grown $Tb_{0.3}Dy_{0.7}Fe_{1.9}$ at high drive levels. *J. Appl. Phys.*, **67**(9), May 1990.

[78] F.T. Calkins. *Design, analysis and modeling of giant magnetostrictive transducers*. PhD dissertation, Iowa State University, Ames, Iowa, 1997.